Research on soliton molecule generation with external independent controllable modulation period and pulse width and its gain-managed nonlinear amplification

Yongmao Wang(王永茂), Yuchao Wang(王玉超), Ze Li(李泽), and Zhiguo Lv(吕志国)*

School of Physical Science and Technology, Inner Mongolia University, Hohhot 010021, China
*Corresponding author. Email: lvzhiguo@imu.edu.cn

Abstract: Soliton molecules offer significant practical advantages in high-speed optical communications and precision spectroscopy. However, owing to limitations inherent in passive generation inside the laser cavity, independently controlling the spectral modulation period and pulse duration remains challenging for a laser based solely on soliton molecules. This work reports the generation and amplification of soliton molecules based on Lyot filtering and gain-managed nonlinear (GMN) amplification, in which the spectral modulation period and pulse duration can be independently and actively tuned outside the laser cavity. The birefringence-based Lyot filter enables precise control over both the spectral modulation period and the inter-pulse separation. GMN amplification effectively suppresses gain narrowing and overcomes the gain-bandwidth limitation, thereby enabling a much broader spectrum and much shorter pulse output. As a principle-based demonstration in our work, the modulation period is varied from 2 nm to 2.7 nm, corresponding to the pulse intervals of 3.68 ps and 3.06 ps, respectively. After GMN amplification, the average powers are amplified to 124.5 mW and 149.7 mW, respectively, and the pulse widths are 154 fs and 164 fs, respectively. Additionally, we conclude that GMN amplification does not alter the inherent spectral modulation period and pulse interval of soliton molecules. Under GMN amplification, soliton molecules also exhibit the same amplification characteristics as conventional pulses, such as asymmetric spectral broadening toward longer wavelengths and the ability to achieve ultrashort pulse durations. To the best of our knowledge, this is also the first demonstration of the pulse dynamics of soliton molecules under GMN amplification.

Keywords: soliton molecule, gain-managed nonlinear amplification, external independent controllable.

PACS:42.55.Xi,42.65.Re,42.65.-k ,42.60.Da

1. Introduction

Soliton molecules have attracted considerable attention owing to their potential applications in long-distance optical communication, optical logic systems, and high-resolution optical technologies[1][2][3]. Soliton molecules represent a fascinating phenomenon in soliton dynamics. The ability of multiple solitons to be energy quantized and bounded together stems from the peak power limited effect in laser resonator, as well as the balance between intra-pulse repulsive and attractive forces related with nonlinear and dispersive effects [4][5][6][7]. Based on the Ginzburg–Landau equation, the first theoretical prediction of soliton molecules was done by Malomed [8], followed by Akhmediev *et al.*, who also obtained soliton molecules using interaction plane method [9]. Subsequently, time-domain soliton molecules were experimentally verified in fiber lasers [10][11][12]. In the most of the reported literatures, researchers have conducted in-depth studies on soliton molecules in fiber lasers using a variety of mode-locking techniques, including nonlinear polarization rotation [13][14][15], nonlinear amplifying mirrors[16], nanomaterials [17][18][19][20] and so on. Although the aforementioned methods can generate stable soliton molecules and are technically mature, their primary limitation is their dependence on passive generation mechanisms, leading to limited system controllability. Soliton molecules generated passively inside the cavity are subject to constraints from pulse properties, coexistence effects, and phase relationships. After offline parameter tuning, they not only disturb the original operating state but also induce variations in repetition rate, spectral profile, and pulse characteristics. Therefore, it is urgent to develop a novel approach that integrates stable soliton-molecule generation with active controllability to overcome these technical challenges. In addition, both the spectral bandwidth and the pulse duration are limited by passive generation due to the finite optical gain or severe nonlinear effects within the gain waveguide structure. Consequently, soliton molecules suffer from low energy, long pulse duration, and narrow spectral bandwidth, and thus do not yet meet the performance requirements for practical applications. Therefore, spectral broadening, energy amplification, and pulse compression are required to enhance the practical applicability of soliton molecules.

GMN amplification overcomes the conventional gain-bandwidth limitation for pulses from conventional mode-locked seed sources, enabling the generation of high-average-power pulses with asymmetric temporal profiles and smooth bell-shaped spectra. Its inherent linear chirp characteristics support direct compression to near Fourier transform-limit pulse duration[21][22][23]. In our prior work, GMN amplification has been utilized to generate pulses with an energy of 8.65 nJ and a duration of 102 fs, covering a 3 dB bandwidth of 67.54 nm with a frequency variable seed source[24]. These results confirm the broad practical applicability of GMN amplification, provide experimental evidence for its reliable operation with different seed sources, and broaden its potential applications in ultrafast fiber lasers. On the basis of the above analysis, GMN amplification of soliton molecules has not yet been experimentally reported. Therefore, this gap offers an opportunity to improve the performance of soliton molecules through spectral broadening, energy amplification, and pulse compression, thereby meeting the requirements for practical applications and opening new avenues for theoretical and experimental studies in this field.

In light of the current state of research, in this work, we propose a novel method for soliton-molecule generation and amplification. Independent external periodic spectral filtering is performed between the seed source and the amplifier. This approach overcomes the limitations of intracavity control. The principle is as follows: a broadband mode-locked pulse passes through a Lyot filter external to the seed source, which is formed by fusion splicing polarization-maintaining (PM) components with a rotational offset between their principal axes. Owing to the birefringence of the PM fiber, the polarization state of the pulse evolves periodically. When a polarizer is placed at the output, the transmitted spectrum exhibits periodic spectral modulation and displays a wavelength-dependent sinusoidal profile. By adjusting the physical length of PM fiber to alter the birefringence delay, spectral modulation period can be actively and precisely tuned outside the cavity conceptually. As the pulse, corresponding to the periodic modulation spectra, passes through an additional bandpass filter, we can select the specific spectrum that with a certain number of transmission peaks through the bandpass filter. After that, the pulse could then be GMN amplified in an active fiber with normal dispersion.

As a proof-of-principle demonstration, we use a bandpass filter with a 10 dB bandwidth of 5 nm to extract two or more adjacent transmission peaks from the modulated spectrum. The modulation period ranges from 2 nm to 2.7 nm, corresponding to pulse intervals of 3.68 ps and 3.06 ps, respectively. After GMN amplification, the average powers and pulse durations are 124.5 mW/154 fs, and 149.7 mW/164 fs, respectively. This experimental method enables the active generation of soliton molecules with an externally and independently controllable modulation period and pulse interval under GMN amplification. We have experimentally demonstrated, for the first time, that soliton molecules also exhibit the same amplification characteristics as conventional pulses under GMN amplification, such as asymmetric spectral broadening toward longer wavelengths and the ability to achieve ultrashort pulse durations. In contrast to previously reported generation techniques for soliton molecules, our approach avoids any complex and cumbersome adjustment of laser cavity parameters, thereby achieving stable generation of soliton molecules with active and flexible control (such as spectral period, pulse interval, and short pulse duration), and provides a new research avenue for generating high-performance soliton molecules with variable spectral period and pulse interval.

2. Numerical simulation

The all-PM Lyot filter is formed by splicing a segment of PM fiber to the pigtail ports of the seed source and the polarizer, and the principal axes of these PM fibers are aligned at specific angles with respect to one another. The structure contains two fusion splices. To better identify the factors influencing the spectral modulation period, Jones matrices are used to simulate the transmission characteristics.

$$E_{\text{out}} = MR(-\theta_2)JR(\theta_1)E_{\text{in}} \quad [1]$$

E_{in} and E_{out} represent the incident light and the output light, respectively. M denotes the polarizer and J represents the PM fiber. $R(\theta_1)$ and $R(-\theta_2)$ correspond to the first splicing angle and the second splicing angle, respectively. To simplify the calculation, the polarizer is set along the fast axis, and these Jones matrixes can be respectively expressed as follows.

$$E_{\text{in}} = \begin{bmatrix}1\\1\end{bmatrix}, M = \begin{bmatrix}1 & 0\\0 & 0\end{bmatrix}, R(\theta) = \begin{bmatrix}cos\,\theta & sin\,\theta\\ -sin\,\theta & cos\,\theta\end{bmatrix}$$

$$J = \begin{bmatrix} exp\left(-j\frac{\pi\Delta n}{\lambda}L_{PMF}\right) & 0 \\ 0 & exp\left(+j\frac{\pi\Delta n}{\lambda}L_{PMF}\right)\end{bmatrix} \quad [2]$$

where λ is the input wavelength, L_{PMF} is the length of PM fiber. θ_1 and θ_2 are the angles of the first and second spliced junctions, respectively. $\Delta n = n_{\text{fast}} - n_{\text{slow}}$ is the fiber birefringence. Let $\theta_1 = \theta_2$, and the relative transmittance can be expressed as follows:

$$T(\lambda) = \cos^2\left(\frac{\pi\Delta n}{\lambda}L_{PMF}\right)\sin^2 2\theta + \cos^2 2\theta \quad [3]$$

According to Eq. [3], the expression for the free spectral range (FSR) can be derived as

$$\text{FSR} \approx \frac{\lambda^2}{\Delta n L_{PMF}} \quad [4]$$

And thus, the FSR is inversely proportional to the length and birefringence of PM fiber.

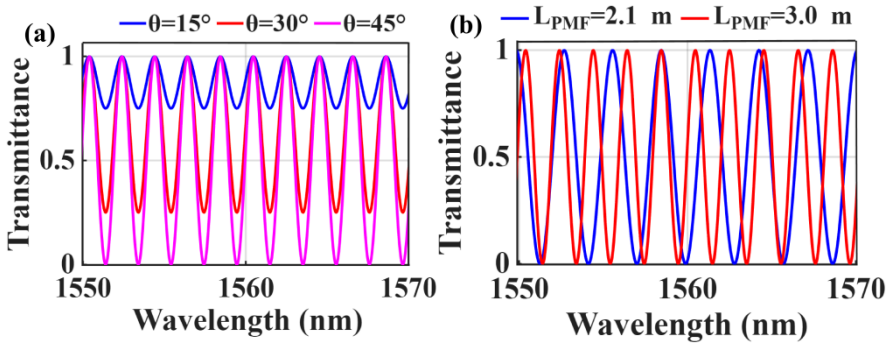


Fig 1. (a)Transmission curves, respectively correspond to 15° (blue), 30° (red), and 45° (purple) splicing angles with the same PMF length of 3 m. (b) Transmission curves, respectively correspond to PMF length of 2.1 m (blue) and 3 m (red) at same splicing angle of 45°.

According to Eq. [3], we conduct numerical simulations with θ and L_{PMF} as variables. The incident wavelength is set to $\lambda = 1565$ nm. Δn is set to 4.0×10^{-4}. When the L_{PMF} is 3 m, the transmission spectra at different splicing angles (θ=15°, 30°, 45°) are respectively shown in Fig.1 (a) with blue, red and purple curves. It is evident that when θ=45° (in this case, the incident linear polarization light E_{in} is

decomposed into two equally intense polarization components), the Lyot filter achieves the maximum modulation depth. Additionally, taking L_{PMF} =2.1 and 3 m as examples, the effect of L_{PMF} on FSR is also presented in Fig.1 (b). In Lyot filter, as the two polarization components are transmitted along the fast and slow axes, respectively, they obtain phase hysteresis relevance with θ and L_{PMF}. Subsequently, as the two polarization components are coherently superimposed on the polarizer, their combined spectrum exhibits periodic modulation characteristics in the frequency domain. According to the numerical simulation, except for the relative intensity between the two polarization components, the modulation characteristics is also related to L_{PMF}, which is inversely proportional to L_{PMF}. These results confirm that the spectral modulation period can be effectively controlled by tailoring the length of PM fiber.

3. Experimental setup

The experimental setup, as shown in Fig. 2, consists of a seed source (an all-PM laser mode-locked by a semiconductor saturable absorber mirror (SESAM)), a fiber filter, a GMN amplifier, and a free-space compressor. The seed source employs a linear cavity configuration. A 976 nm single-mode laser diode (LD) is coupled into the cavity through a 960/1580 nm PM wavelength-division multiplexing hybrid (PM-Tap & WDM hybrid, PM-TWDM), which integrates the functions of a WDM and a coupler. The coupler has a 90:10 coupling ratio, and the 10% port serves as the output. The gain medium is a 0.75-m-long erbium-doped fiber (Nufern, PM-ESF-7/125, designated as EDF1), the other end of which is connected to the SESAM acting as the mode-locker. The seed source has a cavity length of 1.2 m and a repetition rate of 87 MHz, corresponding to a pulse interval of 11.5 ns, as shown in Fig. 3(a). Self-starting mode locking is achieved at a pump power of 91.3 mW with an output power of 2 mW. Fig. 3(b) shows the output spectrum, which is centered at 1565.16 nm with a 3 dB bandwidth of 8.96 nm. The autocorrelation trace is shown in Fig. 3(c), with a pulse width of 341 fs. Fig. 3(d) shows the RF spectrum with a bandwidth of 100 MHz and a resolution bandwidth (RBW) of 10 kHz. Clearly, at a fundamental repetition rate of 87 MHz, the signal-to-noise ratio (SNR) at this fundamental frequency is 65 dB. No spurious frequency components were detected within a 1 GHz bandwidth (see inset),

indicating that the laser system achieves robust single-pulse operation and excellent pulse-to-pulse stability.

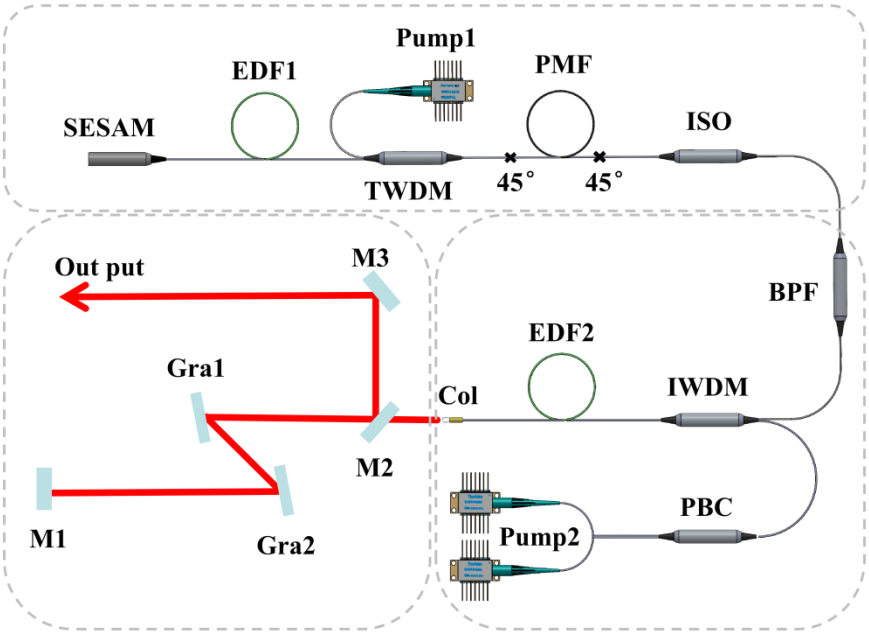


Fig 2. Experimental setup. SESAM, semiconductor saturable absorber mirror. TWDM, tap wavelength-division multiplexing hybrid. PMF, polarization-maintaining fiber. ISO, polarization maintaining isolator. BPF, bandpass filter. IWDM, isolator wavelength-division multiplexer. PBC, polarization beam combiner. Col, collimator. Gra1/Gra2, reflective gratings. M, mirror.

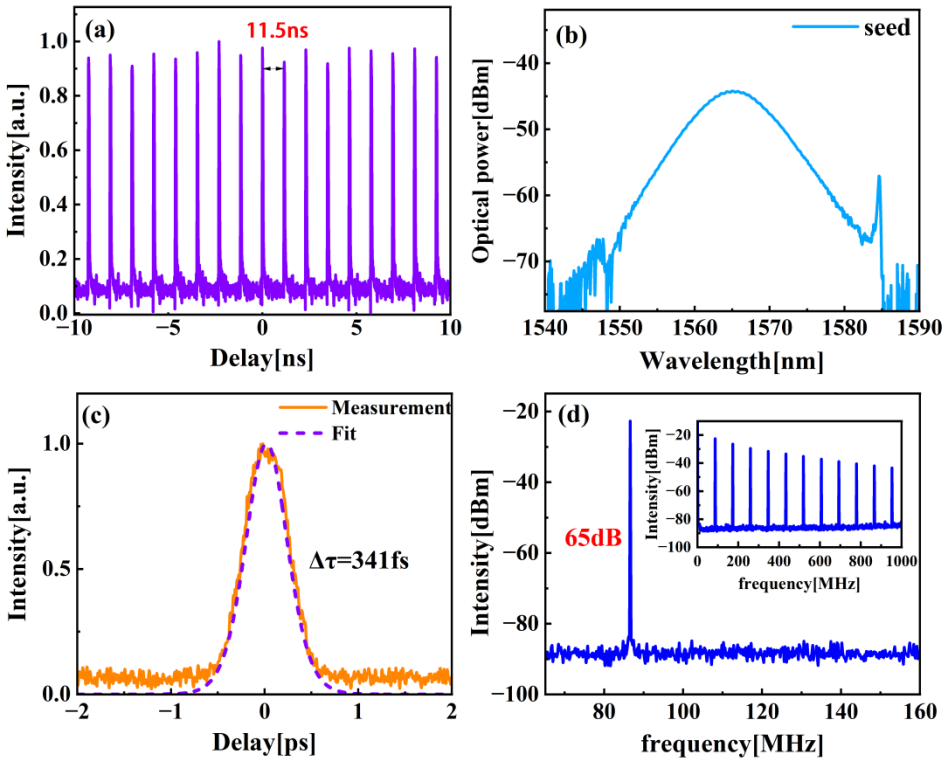


Fig 3. Laser characteristics of seed source: (a) Pulse train. (b) Optical spectrum.(c) autocorrelation (d) RF spectrum.

The Lyot filter consists of a segment of PM-1550 fiber spliced to the pigtail of the seed source with a splice angle of 45° . The other end of the PM fiber is fusion-spliced to the subsequent polarization-maintaining isolator (PM-ISO) at the same angle. Serving as both a polarizer and an isolator, the PM-ISO not only determines the polarization state but also ensures unidirectional propagation, preventing the back-reflected amplified light from perturbing the seed source.

After the Lyot filter, a bandpass filter (BPF) is employed to reshape the spectrum and tailor the pulse duration, thereby facilitating spectral broadening during subsequent amplification. The BPF has a central wavelength of 1560 nm and a 10-dB passband width of 5 nm. At this central wavelength, the BPF selects several periodically modulated transmission peaks from the spectrum of the Lyot-filtered pulses. The number of such transmission peaks is determined by the length of the PM fiber (L_{PMF}).

The filtered pulses are subsequently amplified in a segment of erbium-doped fiber (Nlight Er30-4/125, designated as EDF2). With the EDF2 length optimized to 10 m, the desired GMN pulse evolution is achieved in the normal dispersion regime, enabling

effective spectral broadening as the pump power increases. The maximum pump power of 1.28 W is delivered through a 960/1589 nm polarization-maintaining integrated wavelength-division multiplexer (PM-IWDM, PM-ISO and WDM). After amplification, the amplified pulses are collimated into free space via a fiber collimator. Finally, the pulses are compressed by a pair of reflection gratings (Thorlabs, GR25-0616, G1/G2) with a groove density of 600 lines/mm, achieving a compression efficiency of 41%.The detection instruments include a 5-GHz high-speed real-time oscilloscope (RIGOL, DS70504), an InGaAs photodetector (Electro-Optics Technology, ET-3000, bandwidth > 2 GHz), an optical spectrum analyzer (Yokogawa, AQ6370D), an optical autocorrelator (A.P.E., SM2000), and a power meter (Ophir, PD300-IR).

4. Experimental Results

When L_{PMF} is 3 m, the spectra output from the ISO and the BPF are shown as blue and red lines, respectively, in Fig. 4(a). In addition to the spectral profile remaining unchanged, the incident seed spectrum exhibits periodic spectral modulation due to birefringence modulation in the PM fiber. The experimentally measured spectra are depicted as blue lines in Fig. 4(a2), with a modulation period of 2 nm, which is consistent with the numerical simulation results shown by the purple lines in Fig. 4(a1). The resolution is 0.2 nm. At this stage, the use of the Lyot filter with flexible parameter control facilitates the conversion from conventional solitons to soliton molecules. The measured autocorrelation traces are shown in Fig.4(b). Three peaks are observed with an intensity ratio of approximately 1:2:1, which is a typical temporal signature of a double-pulse soliton molecule. The temporal separation between adjacent pulses remains 3.68 ps, which matches the spectral modulation period calculated from the Fourier transform relation ($c \cdot \Delta T \cdot \Delta\lambda = \lambda^2$). The corresponding pulse duration is 0.996 ps. After the x-axis of Fig. 4(a2) is shortened, as shown in Fig. 4(d), the central wavelength is 1564.87 nm, and the two peaks at this wavelength have equal intensities. The optical spectrum shown in Fig. 4(d), together with the optical autocorrelation trace in Fig. 4(b), indicates that the phase difference between the two

mode-locked solitons is approximately π, and that the bound state is a tightly bound soliton pair. Fig. 4(c) presents the RF spectrum over a span of 100 MHz (60 – 160 MHz) with a resolution bandwidth (RBW) of 10 kHz. Clearly, at a fundamental repetition rate of 87 MHz, the SNR is 60 dB. This demonstrates that the fiber laser exhibits excellent mode-locking stability and minimal pulse energy fluctuations. After the modulated spectrum passes through the BPF, only three transmission peaks centered around 1560 nm are transmitted, as shown by the red curve in Fig. 4(a2). After spectral filtering, the average power decreases to 0.14 mW. Subsequently, the three-peak spectrum undergoes amplification and spectral broadening. Fig. 4(e) presents the measured evolution of the spectral bandwidth and profile as a function of pump power. As the pump power increases, the spectrum broadens asymmetrically while the central wavelength shifts toward longer wavelengths, exhibiting a parabolic intensity distribution consistent with the GMN amplification regime. In terms of morphology, the periodic spectral modulation characteristics are consistently maintained throughout the amplification process, with the same modulation period as the initial three-peak spectrum. With increasing pump power and spectral broadening, the spectral modulation period remains 2 nm. Overall, the spectral evolution during amplification is governed by the GMN mechanism, while the soliton molecules retain their inherent spectral modulation and bound-state characteristics in both spectral and temporal domains. Amplification has no effect on the inherent characteristics of the soliton molecules themselves. We attribute the constant spectral modulation after amplification to the modulation instability (MI) induced spectral shaping. In the four-wave mixing (FWM) process, two pump photons at frequency ω_0 are annihilated and converted into a pair of new photons respectively at frequencies $\omega_0+\Omega$ and $\omega_0-\Omega$, thereby generating new spectral components symmetrically distributed on either side of the center frequency ω_0. Because these newly generated sidebands fall within the gain bandwidth of MI, they are effectively amplified by the parametric gain provided by MI rather than decaying away. The spectral signature of MI in the frequency domain is precisely a pair of symmetric side lobes appearing on either side of the center frequency ω_0, each offset by $\pm\Omega$. In the present experiment, the frequency difference Ω of the input trimodal spectrum corresponds to a wavelength spacing of 2

nm, so both the sideband spacing generated by FWM and the gain peak positions of MI are locked to this beat frequency Ω. The newly created sidebands then act as pump sources themselves, participating in cascaded FWM processes that successively generate higher-order sidebands at $\omega_0 \pm 2\Omega$, $\omega_0 \pm 3\Omega$, and so on, with the spacing between every adjacent order remaining strictly fixed at Ω (2 nm). Consequently, although the spectrum undergoes significant broadening during amplification, the modulation period remains fixed at the initial spectral spacing of 2 nm, resulting in an equidistant, comb-like modulation structure throughout the broadened spectrum. However, we attribute the asymmetry of the measured spectra to GMN amplification. Initially, the spectral evolution is dominated by self-phase modulation with a symmetrical multi-peak distribution (Fig. 4(g)). Furthermore, influenced by GMN amplification, which manifests as short-wavelength absorption and long-wavelength amplification, the pulse spectrum shifts asymmetrically toward longer wavelengths. Therefore, the spectral features shown in Fig. 4(e) result from the combined action of MI and GMN amplification. Both MI-induced spectral reshaping and GMN-related spectral broadening preserve the original modulation period in the significantly broadened spectrum. When the pump power is increased to 1280 mW, the optical spectrum spans from 1542 to 1597 nm with a 10-dB bandwidth of 27.5 nm (measured at 0.2 nm resolution), yielding an average output power of 124 mW. Fig. 4(f) shows the compressed autocorrelation traces corresponding to Fig. 4(e) under different pump powers. Three peaks are observed with an intensity ratio of approximately 1:2:1, which temporal interval in accordance with that of incident pulses. After amplification, the measured compressed pulse durations are 154 fs (1280 mW), 161 fs (1064 mW), 186 fs (895 mW), 234 fs (729 mW), and 263 fs (551 mW), respectively. The peak power after compression at the maximum pump power is 2.5 kW. The system achieves optimal performance when the pump power is 1280 mW. The spectral bandwidth is 14.12 nm (at 3 dB), and the compressed pulse duration is 1.2 times the Fourier transform-limited value, indicating that the linear chirp is efficiently compensated.

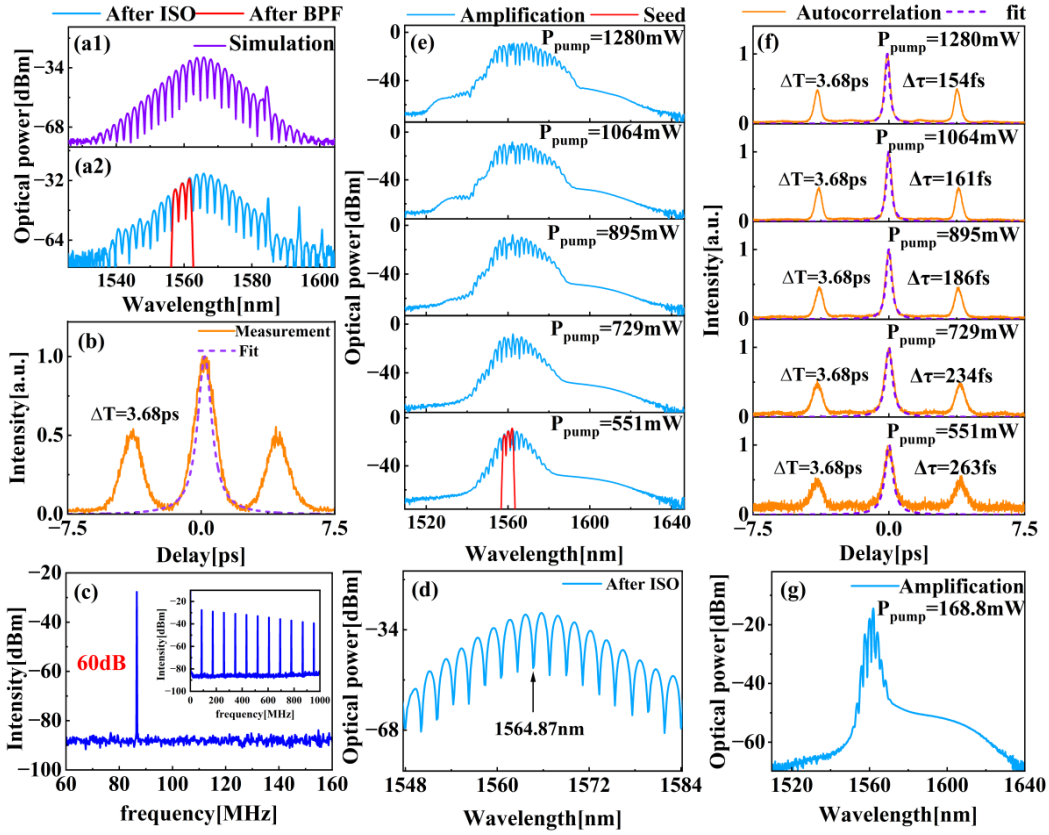


Fig 4 Laser characteristics for $L_{\mathrm{PMF}} = 3\,m$. (a1) Simulated spectra. (a2) Spectra after ISO (blue line),
and BPF (red line). (b) Autocorrelation trace after Lyot filter. (c) RF spectrum after Lyot filter. (d) Spectra after ISO (e) Spectral evolution versus varying pump power. (f) Autocorrelation trace after

Furthermore, we investigate the case with an L_{PMF} of 2.1 m. The spectra sequentially output from the ISO and BPF are shown as blue and red lines, respectively, in Fig. 5(a2). The spectral profile exhibits similar features to that in Fig. 4(a2), but with a modulation period of 2.7 nm. The resolution is also 0.2 nm. After the modulated spectrum passes through the BPF, two transmission peaks centered around 1560 nm are transmitted. Fig. 5(a2) shows the transmitted spectrum as a red line. After the BPF, the average power is 0.19 mW. As shown in Fig. 5(d), after the x-axis of Fig. 5(a2) is scaled, the central wavelength is 1564.47 nm, and the two spectral dips at this central wavelength have equal intensities. The spectrum shown in Fig. 5(d), together with the optical autocorrelation trace in Fig. 5(b), indicates that the phase difference between the two mode-locked solitons is approximately zero, confirming that this bound state is a tightly bound soliton pair. Fig.5(c) displays the radio frequency (RF) spectrum with a bandwidth of 100 MHz. The RF spectrum analyzer has a resolution of 10 kHz. Clearly,

at a fundamental repetition rate of 87 MHz, the signal-to-noise ratio of this RF spectrum is 62 dB. Similar to the case of a 2 nm spectral modulation period, as the pump power increases, the periodic spectral modulation characteristics are consistently maintained throughout the amplification process, with the same modulation period of 2.7 nm. The spectral evolution also results from the combined action of MI and GMN amplification. At the highest pump power, the 10 dB bandwidth reaches 23.04 nm, and the maximum average output power is 124 mW._After amplification, the measured compressed pulse durations are 164 fs (1280 mW), 181 fs (1064 mW), 196 fs (895 mW), 222 fs (729 mW), and 266 fs (551 mW). The peak power after compression at the maximum pump power is 2.7 kW. In the case of dual-peak amplification, the pulse evolution characteristics are essentially consistent with those of the three-peak amplification output in both the temporal and spectral domains. This consistency indicates that GMN amplification preserves the inherent spectral modulation period and temporal separation of soliton molecules, regardless of the number of incident spectral modulation peaks. When the conditions for GMN amplification are satisfied, soliton molecules exhibit the same amplification characteristics as conventional pulses, including asymmetric spectral broadening toward longer wavelengths and the ability to achieve ultrashort pulse durations. To the best of our knowledge, this is the first demonstration of soliton-molecule pulse dynamics under GMN amplification.

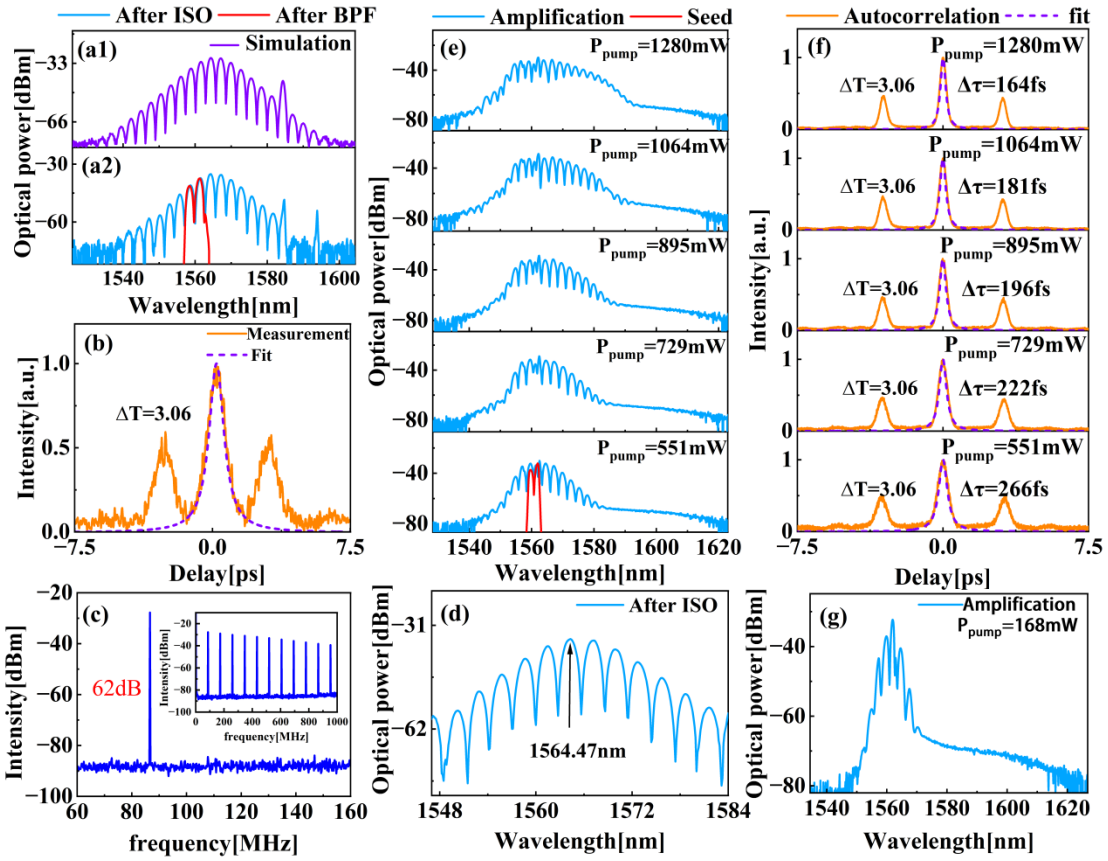


Fig 5. Laser characteristics for $L_{\mathrm{PMF}} = 2.1\,m$. (a1) Simulated spectra. (a2) Spectra after ISO (blue line), and BPF (red line). (b) Autocorrelation trace after Lyot filter. (c) RF spectrum after Lyot filter. (d) Spectra after ISO. (e) Spectral evolution versus varying pump power. (f) Autocorrelation trace after compression. (g) Spectral evolution in initial amplification stage.

When the L_{PMF} is further shortened to 0.75 m, the output spectra of the ISO and the BPF are shown in Fig. 6(a) as the blue and red curves, respectively. The spectral profile is similar to that in Fig. 4(a2), but the modulation period increases to 8.2 nm. When the modulated spectrum passes through the BPF, only one spectral peak at 1560 nm is transmitted. After amplification, the output spectrum at a maximum pump power of 1280 mW is shown in Fig. 6(b). The spectrum retains only the GMN amplification characteristics, with a smooth profile broadened toward longer wavelengths and without periodic modulation, indicating that the spectral filtering effectively suppresses the modulation induced by the SMIF. The spectral bandwidth is 49.75 nm, and the average output power is 153.2 mW. The corresponding pulse duration is measured as 119 fs, as shown in Fig. 6(c). When the BPF transmits only a spectral peak, the frequency-domain spectral modulation present in the initial soliton molecule

is lost, and the time-domain structure of the soliton molecule reduces to a single pulse. Subsequently, as the single pulse undergoes GMN amplification, its output characteristics are entirely dominated by the amplifier gain and nonlinear effects, and thus exhibit only GMN-induced temporal and spectral features. Experimental results indicate that only when two or more transmission peaks are present at the output of the BPF can the temporal and spectral characteristics of the soliton molecule be maintained during GMN amplification.

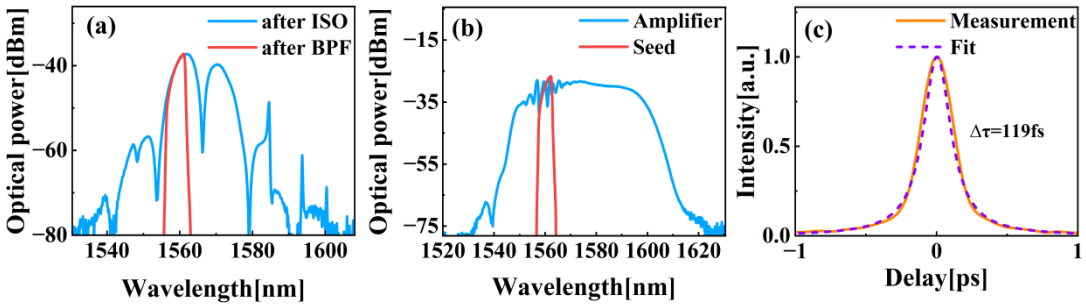


Fig 6. Laser characteristics for L_{PMF}=0.75 *m*. (a) Spectra after ISO (blue line) and BPF (red line). (b) Spectrum after GMN amplification. (c) Autocorrelation trace after compression**.**

5.Conclusion

In summary, we propose a novel method to generate soliton molecules with a controllable spectral modulation period and conduct an in-depth study of their GMN amplification characteristics. Under GMN amplification conditions, these soliton molecules exhibit amplification features similar to those of conventional pulses, including asymmetric spectral broadening toward longer wavelengths and the ability to achieve ultrashort pulse durations. Owing to MI-induced spectral reshaping and GMN-related spectral broadening, the laser characteristics of the soliton molecules remain unchanged after GMN amplification. The modulation period and pulse interval are determined solely by the length of the PM fiber (L_{PMF}) in the Lyot filter. The soliton-molecule features survive GMN amplification only when the BPF transmits two or more peaks. To the best of our knowledge, this work also provides the first demonstration of the pulse dynamics of soliton molecules under GMN amplification.

Our results offer a new research route for generating high-average-power, narrow-pulse-width soliton molecules with variable spectral period and pulse interval.

Acknowledgments

The Natural Science Foundation of Inner Mongolia Autonomous Region of China under Grant 2025MS01009; National Natural Science Foundation of China (NSFC) under Grant 12164030.

Disclosures. The authors declare no conflicts of interest.

References

[1] Zhao F Y, Wang H S, Hu X H, Wang Y S, Zhang W, Zhang T, Sun C D and Yan Z J 2018 Laser Phys. Lett. 15 105101

[2] Li Y Y, Gao B, Ma C Y, Wu G, Huo J Y, Han Y, Wageh S, Al-Hartomy O A, Al-Sehemi A G, Liu L and Zhang H 2023 Laser Photonics Rev. **17** 2200596

[3] Zhang Y S, Feng W J, Wang Q, Ren X Y, Zhang X Y, Zou D F and Li X H 2026 Laser Photonics Rev. **0** e71177

[4] Peng F, Zhang R, Li X H, Zou D F, Huang X W and Zhang G W 2026 Opt. Laser Technol. **197** 114835

[5] Han Y, Gao B, Wen H, Zhu H, Wang T, Chen H, Yang Z and Li Y 2024 Light Sci. Appl. **13** 101

[6] Olivier M and Piché M 2009 Opt. Express 17 405

[7] Han Y, Gao B, Wen H, Zhu H, Wang T, Chen H, Yang Z and Li Y 2024 Light Sci. Appl. 13 101

[8] Malomed B A 1991 Phys. Rev. A 44 6954

[9] Akhmediev N N and Ankiewicz A 1997 Phys. Rev. Lett. 79 4047

[10] Tang D Y, Man W S, Tam H Y and Drummond P D 2001 Phys. Rev. A 64 033814

[11] Grelu P, Belhache F, Gutty F and Soto-Crespo J-M 2002 Opt. Lett. 27 966

[12] Seong N H and Kim D Y 2002 Opt. Lett. 27 1321

[13] Ortaç B, Hideur A, Brunel M, Chédot C, Limpert J, Tünnermann A and Ilday F Ö 2006 Opt. Express 14 6075

[14] Wang Z, Zhan L, Majeed A and Zou Z 2015 Opt. Lett. 40 1065

[15] Zhao L, Tang D and Zhao B 2005 Opt. Commun. 252 167

[16] Yun L and Liu X 2012 IEEE Photonics J. 4512

[17] Wu X, Tang D, Luan X and Zhang Q 2011 Opt. Commun. 284 3615

[18] Gui L, Xiao X and Yang C 2013 J. Opt. Soc. Am. B 30 158

[19] Gui L, Li X, Xiao X, Zhu H and Yang C 2013 IEEE Photonics Technol. Lett. 25 1184

[20] Luo A, Liu H, Zhao N, Zheng X-W, Liu M, Tang R, Luo Z C and Xu W C 2014 IEEE Photonics J. 6 1501508

[21] Chen K, Zheng J, Xu Q, Jiang X, Liu Y, Zhong X and Tang M 2025 Opt. Lett. 50 2129

[22] Xia T, Zhao H, Zhu S, Sun J, Li S and Wei Z 2024 Opt. Express 32 32396

[23] Boulanger V, Olivier M, Trépanier F, Delisle J-C, Pleau L-P and Gagnon S 2023 Opt. Lett. 48 2700

[24] Chen Z, Yang Z, Li Z and Lv Z G 2026 Opt. Express 34 3464